Computers and Geotechnics 79 (2016) 146–158

Contents lists available at ScienceDirect

Computers and Geotechnics

journal homepage: www.elsevier.com/locate/compgeo

Research Paper

Three-dimensional slope reliability and risk assessment using auxiliary random finite element method

Te Xiao [a], Dian-Qing Li [a,*], Zi-Jun Cao [a], Siu-Kui Au [b], Kok-Kwang Phoon [c]

[a] State Key Laboratory of Water Resources and Hydropower Engineering Science, Wuhan University, 8 Donghu South Road, Wuhan 430072, PR China
[b] Institute for Risk and Uncertainty, University of Liverpool, Harrison Hughes Building, Brownlow Hill, Liverpool L69 3GH, United Kingdom
[c] Department of Civil and Environmental Engineering, National University of Singapore, Blk E1A, #07-03, 1 Engineering Drive 2, Singapore 117576, Singapore

ARTICLE INFO

Article history:
Received 18 February 2016
Received in revised form 10 May 2016
Accepted 29 May 2016
Available online 17 June 2016

Keywords:
Slope stability
Reliability analysis
Risk assessment
Spatial variability
Random finite element method
Response conditioning method

ABSTRACT

This paper aims to propose an auxiliary random finite element method (ARFEM) for efficient three-dimensional (3-D) slope reliability analysis and risk assessment considering spatial variability of soil properties. The ARFEM mainly consists of two steps: (1) preliminary analysis using a relatively coarse finite-element model and Subset Simulation, and (2) target analysis using a detailed finite-element model and response conditioning method. The 3-D spatial variability of soil properties is explicitly modeled using the expansion optimal linear estimation approach. A 3-D soil slope example is presented to demonstrate the validity of ARFEM. Finally, a sensitivity study is carried out to explore the effect of horizontal spatial variability. The results indicate that the proposed ARFEM not only provides reasonably accurate estimates of slope failure probability and risk, but also significantly reduces the computational effort at small probability levels. 3-D slope probabilistic analysis (including both 3-D slope stability analysis and 3-D spatial variability modeling) can reflect slope failure mechanism more realistically in terms of the shape, location and length of slip surface. Horizontal spatial variability can significantly influence the failure mode, reliability and risk of 3-D slopes, especially for long slopes with relatively strong horizontal spatial variability. These effects can be properly incorporated into 3-D slope reliability analysis and risk assessment using ARFEM.

1. Introduction

Slope failure (e.g., landslides) is one of the major natural hazards in the world. The occurrence probability and risk of slope failure are related to various geotechnical uncertainties (e.g., [7,23–25,27,30,34,39,44,45]), among which spatial variability of soil properties is one of the most significant uncertainties affecting slope reliability and risk. Previous studies on slope reliability analysis and risk assessment that account for spatial variability mainly focus on two-dimensional (2-D) analysis, such as Griffiths and Fenton [11], Santoso et al. [41], Wang et al. [51], Huang et al. [17], Zhu et al. [54], Li et al. [28,29,33,35], Jamshidi Chenari and Alaie [18]. As shown in Fig. 1, 2-D analysis implicitly assumes infinite length of slope and perfect correlation of soil properties (i.e., infinite spatial autocorrelation distance) in the axial direction. Based on these assumptions, slopes fail along columnar slip surface with infinite length in three-dimensional (3-D) space. This is inconsistent with the actual failure surfaces observed in slope engineering, where slope may fail at any locations of the slope with an irregular and finite slip surface. Thus, it is necessary to investigate 3-D slope reliability analysis and risk assessment, particularly with both 3-D slope stability analysis and 3-D spatial variability modeling of soil properties.

Several studies (e.g., [14,15,20,21,46,47]) have made attempts to assess 3-D slope reliability. These studies can be classified into three categories according to the adopted reliability methods: first-order second-moment method (FOSM), first-order reliability method (FORM), and Monte Carlo Simulation (MCS). Vanmarcke [46,47] pioneered analytical 3-D slope reliability analysis using FOSM and considered the problem as an extension of 2-D slope reliability analysis based on local average and first-passage theories. This work is elegant and valuable. However, it assumed that slope fails along several prescribed cylindrical slip surfaces, which may lead to an overestimated slope reliability since many other potential slip surfaces (e.g., non-cylindrical ones) are ignored. By only accounting for the axial spatial variability, FORM was also applied to 3-D slope reliability analysis [20,21]. If 3-D spatial variability in axial, lateral and vertical directions as shown in Fig. 1 are

* Corresponding author.
E-mail address: dianqing@whu.edu.cn (D.-Q. Li).

http://dx.doi.org/10.1016/j.compgeo.2016.05.024
0266-352X/

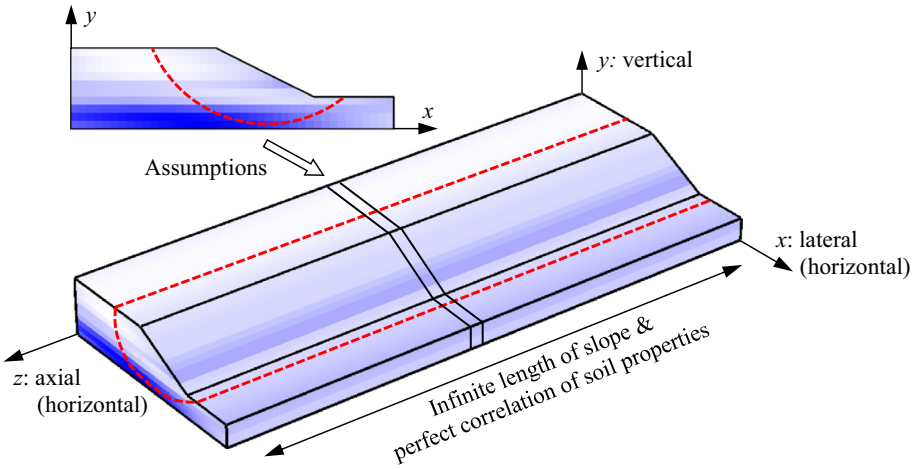

Fig. 1. Assumptions made in 2-D slope reliability analysis.

completely taken into consideration, FORM may encounter computational difficulties, such as high-dimensional problem [43].

Compared with FOSM and FORM, MCS is the most widely-used reliability method for 3-D slope reliability analysis, thanks to the development of random finite element method (RFEM) [11]. The original RFEM, also referred as MCS-based RFEM, incorporates the spatial variability of soil properties into slope reliability analysis using finite-element (FE) analysis and MCS. There are several successful applications of RFEM in reliability analysis of 3-D slope (e.g., [14–16,36]) and slope risk assessment (e.g., [17,31]). RFEM is a rigorous approach since the FE analysis of slope stability can automatically locate the critical slip surface without assumptions on the shape and location. Nevertheless, MCS-based RFEM usually requires intensive computational efforts [19], particularly for detailed 3-D FE models and small probability levels (e.g., slope failure probability $P_f < 10^{-3}$). One simple strategy to address this problem is to adopt a relatively coarse FE model (e.g., the model with coarse FE mesh) in RFEM to improve the computational efficiency of deterministic slope stability analysis. However, coarse FE model may not produce accurate results compared to detailed FE model (e.g., the model with fine FE mesh). For this reason, another RFEM run with detailed FE model is still requisite if more accurate results are required, for example, at later design stages. The computational effort paid for the coarse FE model-based RFEM is thus wasted, and it cannot facilitate the detailed FE model-based RFEM neither, because of no interaction between the two RFEM runs.

In addition, previous studies based on 2-D analysis indicated that the horizontal spatial variability (i.e., lateral spatial variability in the 3-D perspective, see Fig. 1) has minimal influence on slope reliability (e.g., [22,53]). One possible reason is that the lateral scale of slopes is almost in the same order of magnitude as the horizontal autocorrelation distance, namely 20–40 m [38]. In this case, the effect of horizontal spatial variability cannot be captured in 2-D slope reliability analysis. For 3-D slopes, the axial scale can be much larger than the horizontal autocorrelation distance. The effect of horizontal spatial variability on 3-D slope reliability and risk has not been explored systematically.

This paper aims to propose an auxiliary random finite element method (ARFEM) for efficient 3-D slope reliability analysis and risk assessment, and to explore the effect of horizontal spatial variability on 3-D slopes. To achieve these goals, the paper is organized as below. In Section 2, the ARFEM is developed. In Section 3, the modeling of 3-D spatially variable soil properties is presented. The computational effort of ARFEM is discussed in Section 4 and the implementation procedure of ARFEM is summarized in Section 5. A 3-D soil slope example is then presented in Section 6 to demonstrate the validity of ARFEM. Finally, a sensitivity study is carried out to explore the effect of horizontal spatial variability on 3-D slope reliability and risk in Section 7.

2. Auxiliary random finite element method

In slope reliability analysis and risk assessment, the probability of slope failure, P_f, is defined as the probability that the safety factor of slope stability, FS, is smaller than a given threshold fs (e.g., $fs = 1$), namely $P_f = P(FS < fs)$, and the slope failure risk, R, can be defined as the product of P_f and the average failure consequence $\bar{C}$ [17,31]. The computational efficiency and accuracy of P_f and R depend on the deterministic analysis model of slope stability, such as the FE models with coarse and fine FE meshes (referred as coarse and fine FE models, respectively). Both of these two FE models are adopted in ARFEM, which, in turn, constitute two major steps of ARFEM: (1) preliminary analysis using a relatively coarse FE model and Subset Simulation (SS) [3], and (2) target analysis using a fine FE model and response conditioning method (RCM) [2]. They are provided in the following two subsections. To facilitate understanding, subscripts "p" and "t" shall denote the estimates obtained from preliminary and target analyses of ARFEM, respectively.

2.1. Preliminary analysis using coarse FE model and SS

Preliminary analysis aims to efficiently assess slope reliability and risk. For this purpose, coarse FE model and SS are adopted to perform deterministic slope stability analysis and slope reliability analysis at small probability levels, respectively. SS [3,4] stems from the idea that a small failure probability can be expressed as a product of larger conditional failure probabilities for some intermediate failure events, thereby converting a rare event simulation problem into a sequence of more frequent ones. Let $fs_1 > fs_2 > \ldots > fs_{m-1} > fs > fs_m$ be a decreasing sequence of intermediate threshold values, and $F_{p,k} = \{FS_p < fs_k,\ k = 1, 2, \ldots, m\}$ be the intermediate failure events. In implementation, fs_k $(k = 1, 2, \ldots, m)$ are determined adaptively so that the estimates of $P(F_{p,1})$ and $P(F_{p,k}|F_{p,k-1})$, $k = 2, 3, \ldots, m$, always correspond to a common specified value of conditional probability p_0. An SS run with m simulation levels (including one direct MCS level and $m - 1$ levels of Markov Chain MCS) and N samples in each level results in $mN(1 - p_0) + Np_0$ samples in total.

During SS, the sample space is divided into $m+1$ mutually exclusive and collectively exhaustive subsets Ω_k, $k = 0, 1, \ldots, m$, by intermediate threshold values, i.e., $fs_1, fs_2, \ldots, fs_m$, where $\Omega_0 = \{FS_p \geqslant fs_1\}$, $\Omega_k = \{fs_{k+1} \leqslant FS_p < fs_k\}$, $k = 1, 2, \ldots, m-1$, and $\Omega_m = \{FS_p < fs_m\}$. Using the Theorem of Total Probability [1], the $P_{f,p}$ estimated from preliminary analysis can be expressed as

$$P_{f,p} = \sum_{k=0}^{m} P(F_p|\Omega_k)P(\Omega_k) = \sum_{k=0}^{m}\sum_{j=1}^{N_k} I_{p,kj}\frac{P(\Omega_k)}{N_k} \tag{1}$$

where $P(F_p|\Omega_k)$ is the conditional preliminary failure probability given sampling in Ω_k, which can be estimated by $\sum_{j=1}^{N_k} I_{p,kj} \big/ N_k$; $I_{p,kj} = I(FS_{p,j} < fs|\Omega_k)$ is the indicator function of slope failure for j-th sample in Ω_k using coarse FE model; $I_{p,kj} = 1$ if the corresponding FS of j-th sample $FS_{p,j} < fs$, otherwise, $I_{p,kj} = 0$; N_k is the number of random samples falling into Ω_k, and it is equal to $N(1-p_0)$ for $k = 0, 1, \ldots, m-1$, and Np_0 for $k = m$; $P(\Omega_k)$ is the occurrence probability of Ω_k, and it is taken as $p_0^k(1-p_0)$ for $k = 0, 1, \ldots, m-1$, and p_0^k for $k = m$ [50]. In this study, the FS of slope stability is calculated using the shear strength reduction technique [10].

In the context of slope risk assessment, slope failure consequence, C, for each sample should be determined. As pointed out by Huang et al. [17], slope failure consequence depends on the sliding mass volume, V, which can be taken as an equivalent index to quantify the slope failure consequence for simplicity. Analogous to the estimation of $P_{f,p}$, slope failure risk, R_p, in preliminary analysis can also be estimated as

$$R_p = \sum_{k=0}^{m}\sum_{j=1}^{N_k} C_{p,kj}\frac{P(\Omega_k)}{N_k} = \sum_{k=0}^{m}\sum_{j=1}^{N_k} I_{p,kj}V_{p,kj}\frac{P(\Omega_k)}{N_k} \tag{2}$$

where $C_{p,kj}$ and $V_{p,kj}$ are the failure consequence and sliding mass volume corresponding to j-th sample in Ω_k based on coarse FE model, respectively. It can be proved [31] that Eq. (2) is equal to the conventional definition of R, namely, $R = P_f \times \bar{C}$. Herein, failure consequence is evaluated by $C_{p,kj} = I_{p,kj} \times V_{p,kj}$ because it is associated with the occurrence of slope failure. Specifically, failure consequence is represented by the sliding mass volume if slope fails (i.e., $I_{p,kj} = 1$); otherwise, no failure consequence should be considered. In this study, the sliding mass is identified by k-means clustering method [17] based on the node displacements obtained from the FE analysis. In addition to V, the sliding mass length, L, is also taken into consideration to investigate the slope failure mechanism. If there is only one sliding mass along the axis of slope, L is defined as the maximum axial length of the sliding mass; otherwise, L is estimated as the sum of axial lengths of all sliding masses, which might occur when the axial spatial variability of soil properties is strong.

Although $P_{f,p}$ and R_p obtained using coarse FE model are approximate, preliminary analysis can be finished with acceptable computational effort in practice and provides valuable information and insights (e.g., Ω_k, $k = 0, 1, \ldots, m$, and random samples in these subsets) for understanding the slope stability problem. How to incorporate such information and insights into the more realistic fine FE model-based reliability analysis has not been explored in the literature. RCM [2] opens up a possibility to link these two types of reliability analyses. It is adopted in ARFEM to incorporate the information generated from the coarse FE model-based preliminary analysis into the fine FE model-based target analysis, so as to obtain the refined and consistent estimates of P_f and R efficiently.

2.2. Target analysis using fine FE model and RCM

RCM makes use of the information (i.e., random samples in different subsets) about the problem generated using an approximate solution (e.g., the coarse FE analysis) to achieve efficient and consistent reliability estimates with an accurate solution (e.g., the detailed FE analysis). Note that samples in their close neighborhood will have similar performances [40]. Taking advantage of this property, it is reasonable to select a part of samples as the representative samples in small sample space, which is referred as the sub-binning strategy in RCM [2]. By this way, Ω_k can be further divided into N_s sub-bins Ω_{kj}, $j = 1, 2, \ldots, N_s$, which are ranked in a descending order according to FS_p values estimated from preliminary analysis and have the same number of random samples. In each Ω_{kj}, one of N_k/N_s samples is randomly selected as the representative sample to judge whether Ω_{kj} belongs to target failure domain or not, as shown in Fig. 2 schematically. Since Ω_{kj}, $j = 1, 2, \ldots, N_s$, are mutually exclusive and collectively exhaustive sub-bins of Ω_k, the target slope failure probability, $P_{f,t}$, can be expressed as

$$\begin{aligned} P_{f,t} &= \sum_{k=0}^{m} P(F_t|\Omega_k)P(\Omega_k) = \sum_{k=0}^{m}\sum_{j=1}^{N_s} P(F_t|\Omega_{kj})P(\Omega_{kj}) \\ &= \sum_{k=0}^{m}\sum_{j=1}^{N_s} I_{t,kj}\frac{P(\Omega_k)}{N_s} \end{aligned} \tag{3}$$

where $P(\Omega_{kj}) = P(\Omega_k)/N_s$ due to the equal division; $P(F_t|\Omega_k)$ and $P(F_t|\Omega_{kj})$ are conditional target failure probabilities given sampling in Ω_k and Ω_{kj}, respectively; $P(F_t|\Omega_{kj})$ can be estimated by $I_{t,kj} = I(FS_t < fs|\Omega_{kj})$, which is the indicator function of slope failure for the representative sample in Ω_{kj} using fine FE model; $I_{t,kj} = 1$ if the corresponding $FS_t < fs$, otherwise, $I_{t,kj} = 0$. Similarly, the target slope failure risk, R_t, can be written as

$$R_t = \sum_{k=0}^{m}\sum_{j=1}^{N_s} C_{t,kj}\frac{P(\Omega_k)}{N_s} = \sum_{k=0}^{m}\sum_{j=1}^{N_s} I_{t,kj}V_{t,kj}\frac{P(\Omega_k)}{N_s} \tag{4}$$

where $C_{t,kj}$ and $V_{t,kj}$ are the failure consequence and sliding mass volume corresponding to the representative sample in Ω_{kj} based on fine FE model, respectively.

Note that Eqs. (3) and (4) are respective analogues of Eqs. (1) and (2). Using the sub-binning strategy, only $(m+1)N_s$ fine FE analyses are required for estimating $P_{f,t}$ and R_t in Eqs. (3) and (4). This number is much smaller than that (i.e., $mN(1-p_0) + Np_0$) required for directly performing SS based on fine FE model. The computational effort is substantially reduced by incorporating the information generated using SS and coarse FE model in preliminary analysis. It can be shown that the estimates are asymptotically unbiased [2]. This means the results (i.e., $P_{f,t}$ and R_t) obtained from target analysis of ARFEM converge to those obtained from directly performing MCS or SS based on fine FE model.

2.3. Statistical analysis, CDF, and CRF

This subsection makes use of the random samples to evaluate the statistics of FE responses (i.e., FS, V and L) in ARFEM, among which the mean and variance are of great interest to engineers. Since the samples fall in different sample space with different probability weights, the mean and variance should be evaluated using a weighted summation. Let X denote the FE response (e.g., FS, V and L). The mean, $E(X)$, and variance, $D(X)$, of X can be expressed as

$$E(X) = \sum_{i=1}^{n} X_i w_i \Big/ \sum_{i=1}^{n} w_i \tag{5a}$$

$$D(X) = \sum_{i=1}^{n} X_i^2 w_i \Big/ \sum_{i=1}^{n} w_i - [E(X)]^2 \tag{5b}$$

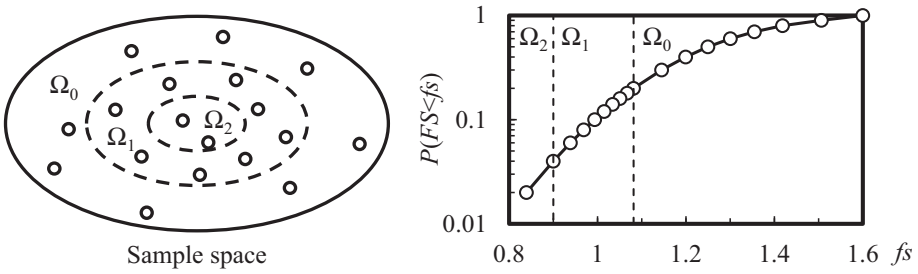

(a) SS using coarse FE model

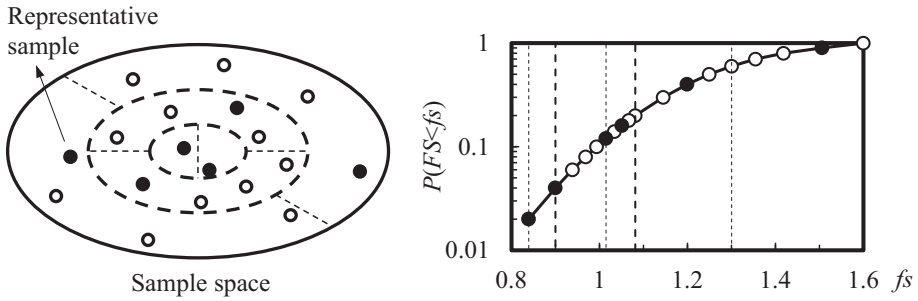

(b) Sub-binning and selection of representative samples in each subset

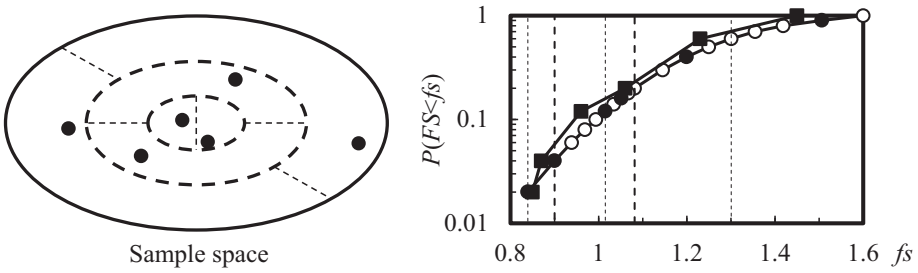

(c) RCM using fine FE model

Fig. 2. Schematic diagram of SS and RCM ($N = 10$, $p_0 = 0.2$, $m = 2$, $N_s = 2$) (modified from Li et al. [32]).

where w_i is the probability weight of i-th selected sample, which is taken as $P(\Omega_k)/N_k$ and $P(\Omega_k)/N_s$ for samples in Ω_k in preliminary and target analyses, respectively; n is the number of samples used in analysis. If the statistical analysis is performed on the whole sample space, n is the total sample size (i.e., $mN(1-p_0)+Np_0$ in preliminary analysis and $(m+1)N_s$ in target analysis), and $\sum_{i=1}^{n} w_i = 1$. If it is performed on the failure space only, n is the failure sample size (i.e., $n_{f,p}$ and $n_{f,t}$ for preliminary and target analyses, respectively), and $\sum_{i=1}^{n} w_i$ is then equal to $P_{f,p}$ for preliminary analysis and $P_{f,t}$ for target analysis.

Likewise, P_f and R (see Eqs. (1)–(4)) can also be considered as the weighted summation of the indicator function of slope failure and the failure consequence, respectively, over the whole sample space. Although samples used in ARFEM are generated according to a predefined fs (e.g., $fs = 1$), they can be used for evaluating P_f and R at any fs values without additional calculation. It only needs to determine the failure samples according to different fs values and to update the indicator functions of slope failure in Eqs. (1)–(4). The variation of P_f as a function of fs can be described by the cumulative distribution function (CDF) of FS. Similarly, an analogue of CDF for slope risk assessment is defined in this work, namely the cumulative risk function (CRF) of FS, which describes the variation of R as a function of fs. The CDF and CRF reflect the slope failure probability and risk at different safety levels. This will be further demonstrated through the illustrative example later.

As mentioned previously, $mN(1-p_0)+Np_0$ random samples are generated in preliminary analysis and $(m+1)N_s$ of them are selected for target analysis. This necessitates the same sample space in the two analyses so that random samples generated in preliminary analysis can be directly used in target analysis. When the spatial variability is considered in FE analysis, it can be modeled as a random field [48]. The random field is usually discretized according to the FE mesh to obtain values of soil properties in each element for the FE analysis, e.g., mid-point method [31,32] and local average subdivision method [14,15]. Hence, the random field realized in a coarse FE mesh has less random variables than those generated in a fine FE mesh. This renders difficulty in using random samples, which are generated during preliminary analysis, in target analysis. To address this problem, expansion optimal linear estimation (EOLE) approach [26] is adopted in ARFEM for 3-D spatial variability modeling, which is briefly introduced in the following section.

3. EOLE for 3-D spatial variability modeling

EOLE [26,42,49] is adopted in ARFEM for the following two reasons: (1) the random field realization at the location of the FE mesh can be estimated according to the random field grid, which makes it possible to employ a set of random field grid that differs from the FE mesh; (2) EOLE is computationally efficient and can be easily extended from 2-D to 3-D [42]. In the context of EOLE, a stationary lognormal random field, $S(x)$, of the uncertain soil parameter S (e.g., undrained shear strength, S_u) can be written as

$$S(x) = \exp\left[\mu + \sum_{i=1}^{r} \frac{\zeta_i}{\sqrt{\lambda_i}} \Phi_i^T \Sigma_{x\chi}\right] \tag{6}$$

where x and χ are the coordinates in FE mesh and random field grid, respectively; μ is the mean value of $\ln(S)$; $\zeta = [\zeta_1, \zeta_2, \ldots, \zeta_r]^T$ is a standard normal random vector with independent components; r is the number of truncated terms, which is determined by the required accuracy of random field discretization (e.g., [49]); λ_i and Φ_i ($i = 1, 2, \ldots, r$) are the respective eigenvalues and eigenvectors of the covariance matrix, $\Sigma_{\chi\chi}$ of $\ln(S)$ associated with random field grid, i.e., $\Sigma_{\chi\chi}\Phi_i = \lambda_i\Phi_i$; $\Sigma_{x\chi}$ is the optimal linear estimation matrix linking the FE mesh to the random field grid. The autocorrelation coefficients, ρ, in $\Sigma_{\chi\chi}$ and $\Sigma_{x\chi}$ can be calculated from a prescribed autocorrelation function. Consider, for example, the squared exponential autocorrelation function, by which ρ is calculated as

$$\rho = \exp\left[-\left(\frac{\Delta x}{l_h}\right)^2 - \left(\frac{\Delta y}{l_v}\right)^2 - \left(\frac{\Delta z}{l_h}\right)^2\right] \tag{7}$$

where Δx, Δy and Δz are the lateral, vertical and axial distances between two different locations, respectively (see Fig. 1); l_h and l_v are the horizontal and vertical autocorrelation distances, respectively. Eq. (7) assumes that the horizontal spatial variability is isotropic in the lateral and axial directions.

Fig. 3 shows an example of a random field realization for different FE meshes using EOLE. The random field is first generated on the random field grid as shown in Fig. 3(a) which is determined according to the accuracy of random field mapping, e.g., two points within an autocorrelation distance [42]. The random field realization is then mapped onto three different FE meshes (Fig. 3(b)–(d)). The number of random variables remains unchanged during the random field mapping, thus not relying on the FE mesh. This property of EOLE is pivotal for the success of ARFEM.

4. Computational effort of ARFEM

The computational effort of ARFEM consists of two parts. The first part is for the evaluation of $mN(1 - p_0) + Np_0$ coarse FE analyses in preliminary analysis, and the second part is for the evaluation of $(m + 1)N_s$ fine FE analyses in target analysis. Let ξ denote the ratio of the computational effort using coarse FE model over that using fine FE model. The total computational effort of ARFEM can be expressed in terms of the equivalent number, N_T, of 3-D slope stability analysis using fine FE model as

$$N_T = (m + 1)N_s + \xi[mN(1 - p_0) + Np_0] \tag{8}$$

The value of ξ depends on the FE models adopted in the calculation. When ξ is relatively small, which means that the coarse FE analysis is much more efficient than the fine FE analysis, the computational effort of ARFEM mainly comes from that used for $(m + 1)N_s$ fine FE analyses in target analysis, which relies on N_s. Typically, N_s is small compared with N.

To further improve the efficiency, parallel computing strategy can be introduced into ARFEM for both deterministic 3-D FE analysis and uncertainty propagation (i.e., SS and RCM). Although the computational efforts of parallel computing and serial computing are equal in terms of sample size, parallel computing can reduce computational time because more computational power is utilized simultaneously. Samples from different Markov chains (i.e., Np_0) can be parallelized for SS, and all selected samples (i.e., $(m + 1)N_s$) can be parallelized for RCM because they have been determined before the target analysis.

5. Implementation procedure

Fig. 4 shows the implementation procedure of ARFEM for 3-D slope reliability analysis and risk assessment. The procedure mainly consists of five steps:

(1) Determine statistics (e.g., mean, standard deviation, and autocorrelation distance), autocorrelation functions and probability distributions of soil properties, and characterize slope geometry.
(2) Perform preliminary analysis using SS with coarse FE model, during which $mN(1 - p_0) + Np_0$ random samples are generated and Ω_k ($k = 0, 1, \ldots, m$) are progressively determined based on the FS_p values. The results of slope reliability and risk (i.e., $P_{f,p}$ and R_p) are calculated using Eqs. (1) and (2), respectively.
(3) Divide Ω_k ($k = 0, 1, \ldots, m$) into N_s equal sub-bins Ω_{kj} ($j = 1, 2, \ldots, N_s$). In each Ω_{kj}, one sample is selected randomly, leading to a total of $(m + 1)N_s$ selected samples.
(4) Perform target analysis using RCM with fine FE model and the $(m + 1)N_s$ samples selected in Step (3). The results of slope reliability and risk (i.e., $P_{f,t}$ and R_t) are refined using Eqs. (3) and (4), respectively.

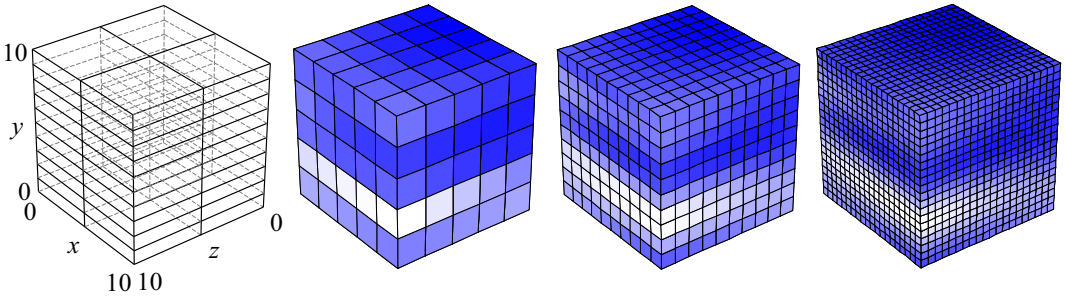

(a) Random field grid (l_h = 10m, l_v = 2m) (b) FE mesh I (mesh size = 2m) (c) FE mesh II (mesh size = 1m) (d) FE mesh III (mesh size = 0.5m)

Fig. 3. Identical random field realization mapped onto different FE meshes using EOLE.

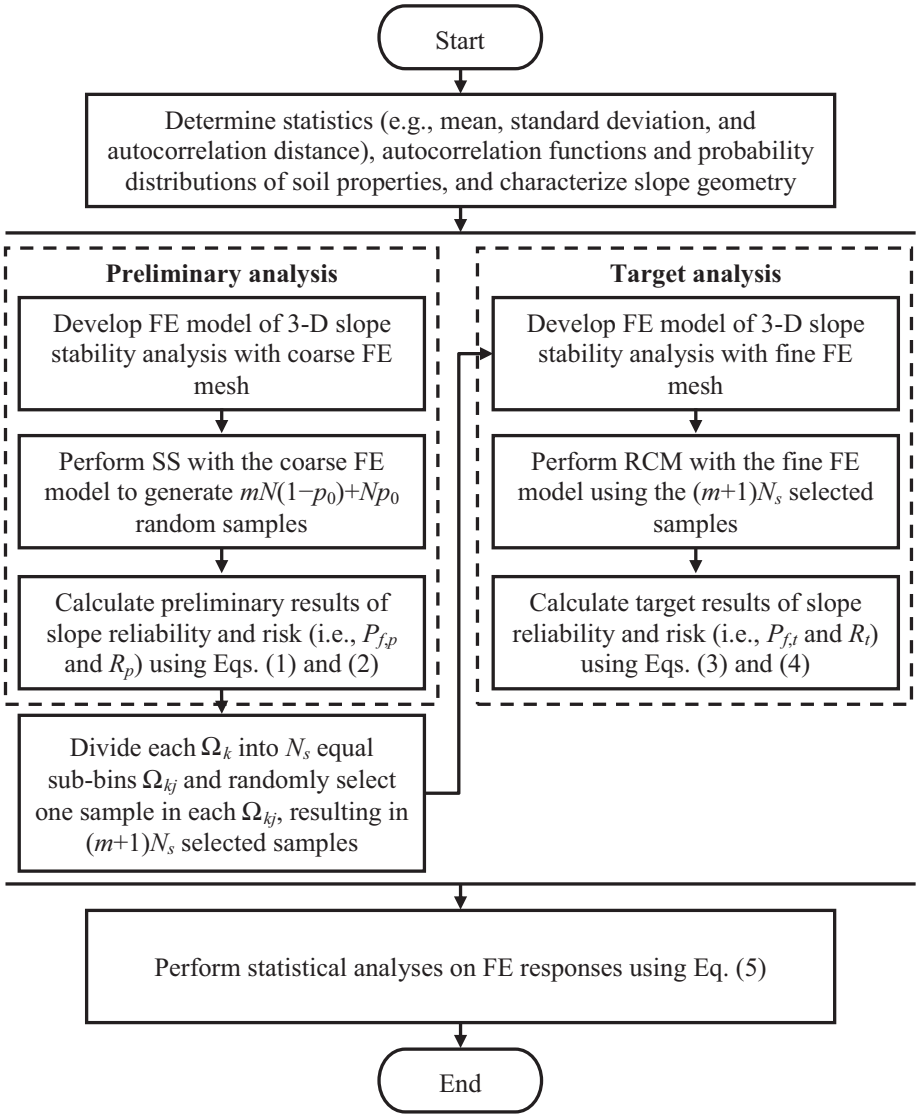

Fig. 4. Implementation procedure of ARFEM for 3-D slope reliability and risk assessment.

(5) Carry out statistical analyses on FE responses using Eq. (5) to obtain their respective statistics.

Although the abovementioned implementation procedure is somewhat more complicated and non-straightforward than MCS-based RFEM, ARFEM can be developed as a user-friendly toolbox and be implemented in a non-intrusive manner [31,32]. By this means, the deterministic slope stability analysis is deliberately decoupled from the uncertainty modeling and propagation. A thorough understanding of ARFEM is always advantageous but not a prerequisite for engineers to use the toolbox. They only need to focus on the deterministic slope stability analysis that they are more familiar with, i.e., developing the coarse and fine FE models for 3-D slope stability analysis in commercial FE software packages (e.g., Abaqus [9]). The toolbox will repeatedly invoke the FE models to calculate *FS* using the shear strength reduction technique and to evaluate *V* and *L* based on sliding mass identification, and will return the preliminary and target results of slope reliability and risk as outputs. This facilitates the practical application of ARFEM in slope reliability and risk assessment.

6. Illustrative example

For illustration, this section applies ARFEM to evaluating the failure probability and risk of a 3-D soil slope. As shown in Fig. 5, the slope has a height (H) of 6 m, a slope angle (α) of about 26.6°, and a length (B) of 100 m. Two FE models are developed in Abaqus, as shown in Fig. 6. The FE mesh size measures 2 m × 2 m × 5 m for the coarse FE model and 1 m × 1 m × 1 m for the fine one. In both models, the bottom (y = 0 m), front (z = 100 m) and back (z = 0 m) sides of slope are fully fixed, and the left (x = 0 m) and right (x = 40 m) sides are constrained by vertical rollers. For soil property, the elastic-perfectly plastic constitutive model with Mohr-Coulomb failure criterion is used in both FE analyses.

Undrained shear strength, S_u, is considered to be lognormally distributed with mean of 30 kPa and coefficient of variation (COV) of 0.3. The spatial variability of S_u is modeled using the squared exponential autocorrelation function with horizontal and vertical autocorrelation distances of 20 m and 2 m, respectively. More actual information on spatial variability of soil properties can be inferred from the site investigation (e.g., [5,6,8,37,52]).

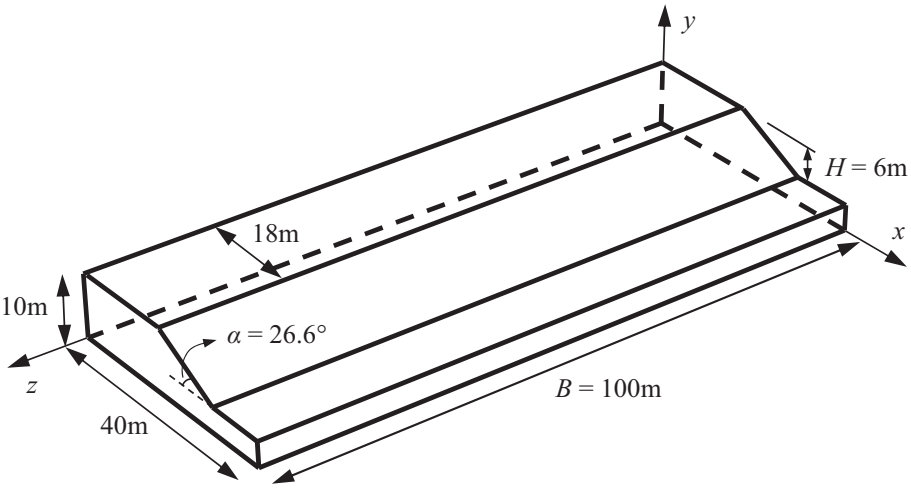

Fig. 5. Geometry of slope example.

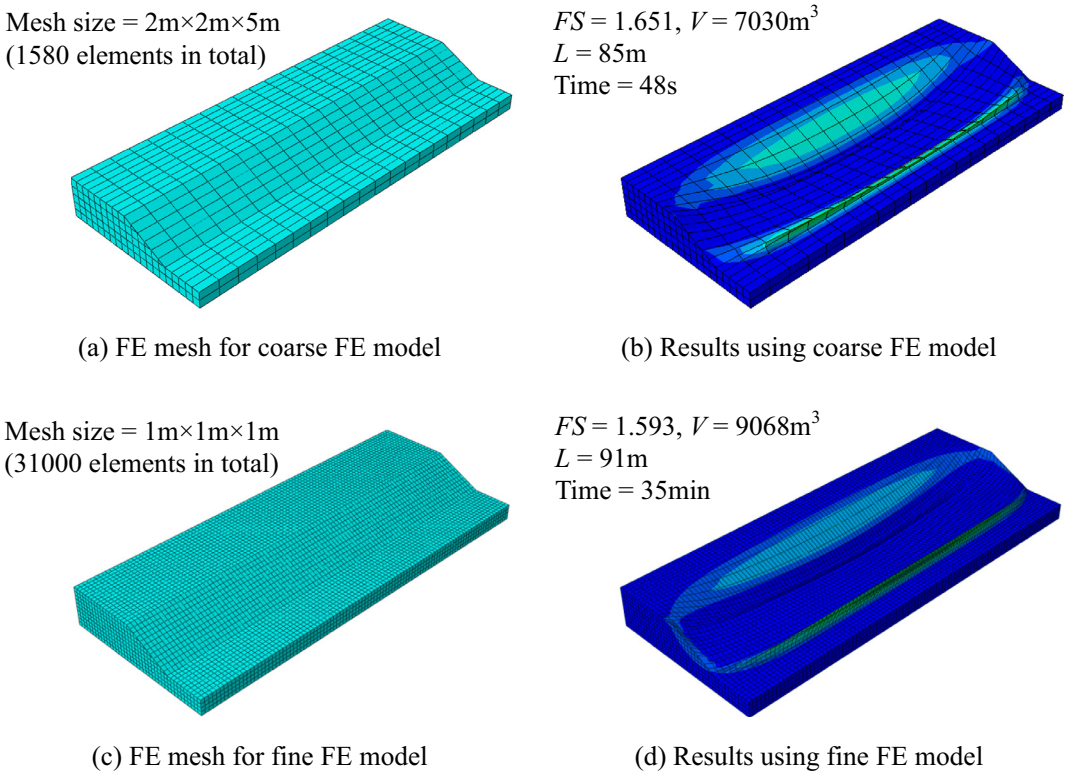

Fig. 6. Coarse and fine FE models and deterministic analysis results.

The unit weight, Young's modulus and Poisson's ratio of soil are 20 kN/m^3, 100 MPa and 0.3, respectively. Note that, the Poisson's ratio has minimal influence on the calculated *FS* in slope stability analysis as pointed out by Griffiths and Lane [10] and Griffiths and Marquez [12]. Although a value of approximately 0.5 for the Poisson's ratio in undrained condition would be most appropriate, a value of 0.3 is adopted in this study, which is commonly used in RFEM-based probabilistic slope stability analysis (e.g., [15,16,36]).

Fig. 6 shows the results of deterministic slope stability analysis based on the mean value of S_u. The failure modes (i.e., critical slip surfaces) identified by the two models are similar and nearly cylindrical. Their sliding mass lengths are almost the same as the slope length. These results appear to be similar to that in 2-D analysis, namely, sliding along the whole slope length from the 3-D perspective. This is because the slope is relatively long and soil is homogeneous without considering spatial variability, which basically satisfies the assumptions adopted in 2-D analysis. The *FS*, *V* and *L* calculated by the coarse FE model are 1.651, 7030 m^3 and 85 m, respectively, while they are 1.593, 9068 m^3 and 91 m for the fine FE model, respectively. The coarse FE model slightly overestimates *FS*, which is consistent with the observation reported by Griffiths and Marquez [12], and underestimates *V* and *L*. This may lead to unconservative estimates of P_f and *R* in probabilistic slope stability analysis. Since the coarse FE model is much more efficient than the fine FE model (i.e., 48 s vs. 35 min), they are adopted to perform preliminary and target analyses in ARFEM, respectively.

6.1. Comparison between 2-D and 3-D slope stability analyses

As can be seen from the above results, the failure mechanism of a 3-D homogeneous slope is similar to that of a 2-D slope. However, soils are typically heterogeneous in geotechnical practice, which can be partially described by spatial variability. Taking this into consideration, this subsection compares 2-D and 3-D slope stability analyses in spatially variable soils.

A typical random field realization of the slope is shown in Fig. 7 (a). The corresponding *FS* of 3-D slope stability analysis calculated by the fine FE model is 0.741, which implies the slope fails. Its slip surface is nearly spherical with a small sliding mass length (i.e., 24 m) located from 19.5 m to 43.5 m in the axial direction. The 3-D heterogeneous slope considering spatial variability of soil properties models real slope failure event more realistically than the 3-D homogeneous slope in terms of the shape, location and length of slip surface. A series (i.e., 100) of cross sections are extracted from the 3-D realization to perform 2-D FE analyses. As shown in Fig. 7, the 2-D *FS* values and slip surfaces vary along the axis of slope. The location of the failed cross sections is from 10.5 m to 48.5 m, whose length is larger than the 3-D sliding mass length. It is also interesting to find that the location (i.e.,

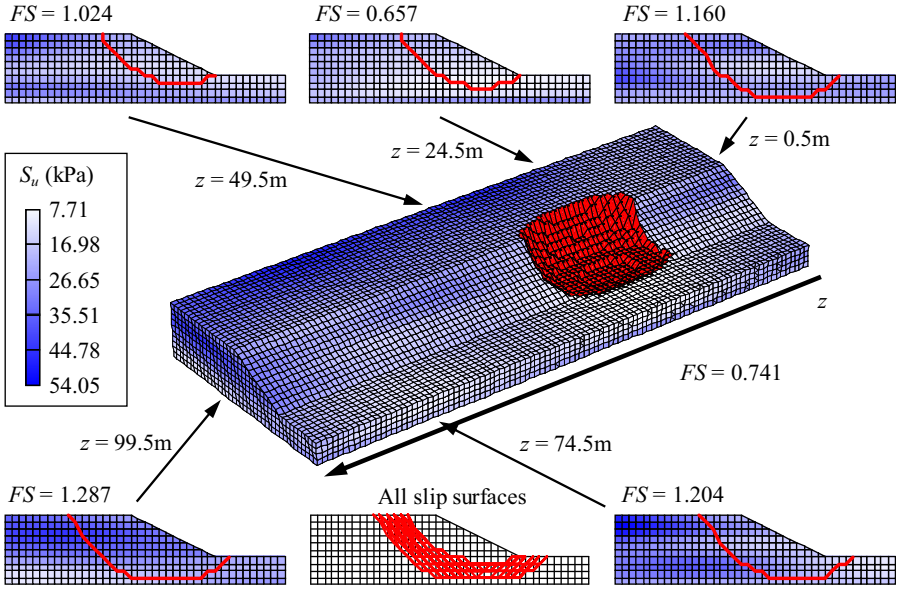

(a) Slip surfaces for 2-D and 3-D analyses

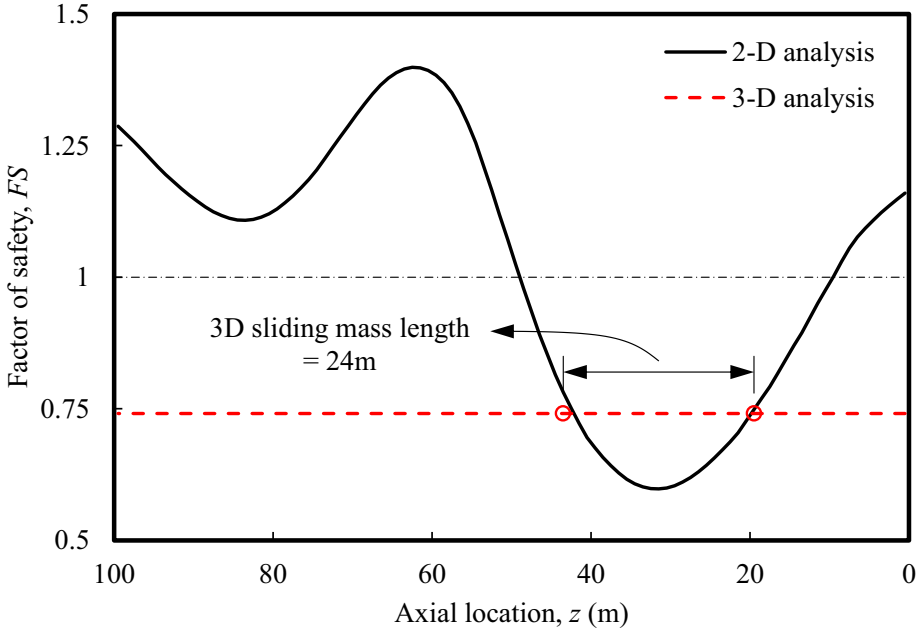

(b) Factor of safety for 2-D and 3-D analyses

Fig. 7. Results of 2-D and 3-D analyses for a typical random field realization.

19.5 m $\leqslant z \leqslant$ 42.5 m) where 2-D *FS* values are smaller than the 3-D *FS* is comparable with the sliding location (i.e., 19.5 m $\leqslant z \leqslant$ 43.5 m) in 3-D slope stability analysis in this example, as shown in Fig. 7(b). Although 2-D analysis could be more conservative than 3-D analysis based on the cross section with minimal 2-D *FS*, the location of the 3-D critical slip surface remains unknown if the 3-D analysis is not performed. Similar discussion can also be found in Griffiths and Marquez [13]. Compared with 2-D slope probabilistic analysis, 3-D slope probabilistic analysis can properly consider horizontal spatial variability in both lateral and axial directions, and automatically locate the critical slip surface with the help of FE analysis. They are crucial to slope risk assessment as illustrated in the following subsections.

6.2. Reliability analysis and risk assessment using ARFEM

To estimate the P_f and R for the slope example, one ARFEM run is performed with $m = 4$, $N = 500$, and $p_0 = 0.1$ in preliminary analysis using the coarse FE model (i.e., Fig. 6(a)) and $N_s = 25$ in target analysis using the fine FE model (i.e., Fig. 6(c)).

Table 1 summarizes the results of P_f and R for $fs = 1$. In preliminary analysis, the sample space is divided into five subsets Ω_k, $k = 0, 1, \ldots, 4$, in a descending order of FS_p values evaluated using the coarse FE model. These subsets contain 450, 450, 450, 450, and 50 random samples, respectively. Among them, 392 samples in Ω_3 and 50 samples in Ω_4 are identified as failure samples for $fs = 1$. Based on these failure samples and their sliding mass volumes, $P_{f,p}$ and R_p are estimated as 8.84×10^{-4} and 1.77 m^3, respectively. The preliminary analysis with 1850 coarse FE analyses requires about 7 h by parallel computing on a desktop computer with 8 GB RAM and one Intel Core i7 CPU clocked at 3.4 GHz. Twenty five samples in each subset are then randomly selected for target analysis. As shown in Table 1, using the fine FE model, the target failure probabilities in Ω_2 and Ω_3 are refined from 0/450 and 392/450 to 5/25 and 25/25, respectively. The values of $P_{f,t}$ and R_t are refined as 2.80×10^{-3} and 7.09 m^3, respectively, which are almost three and four times larger than the preliminary estimates (i.e., 8.84×10^{-4} and 1.77 m^3), respectively. Although only 125 fine FE analyses are performed in target analysis, its computational time (about 27 h on the same computer using parallel computing) is much longer than that for preliminary analysis. In total, approximate 34 h (or 1.4 days) is required using ARFEM for the slope example.

Fig. 8 shows the variation of P_f and R with *fs* (i.e., CDF and CRF) obtained from the preliminary and target analyses in ARFEM. For all *fs* values, both P_f and R obtained from preliminary analysis are underestimated, as predicted in deterministic slope stability analysis. Hence only using coarse FE model in RFEM will lead to unconservative design of slopes. The shape of CRF is quite similar to that of CDF for the slope example. This indicates that the average consequence of slope failure (i.e., $\bar{C} = R/P_f$) is relatively insensitive to slope safety level (i.e., *fs*) compared with P_f and R. The observation is consistent with that in 2-D slope risk assessment [31].

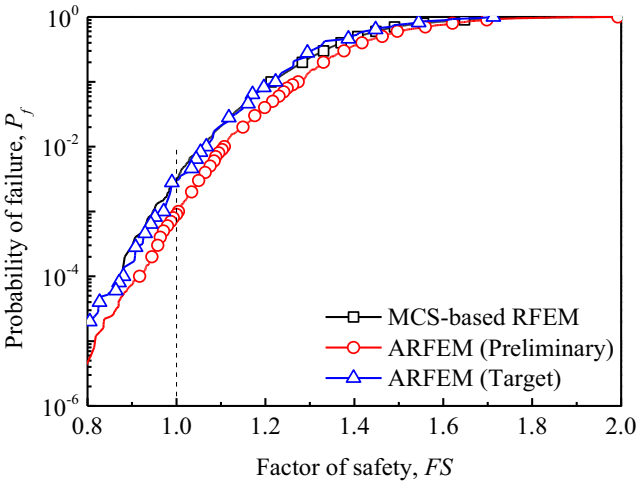

(a) Cumulative distribution function (CDF)

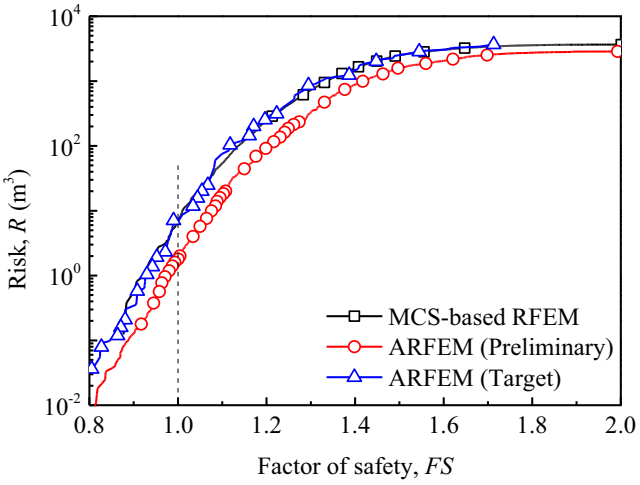

(b) Cumulative risk function (CRF)

Fig. 8. CDFs and CRFs obtained from MCS-based RFEM and ARFEM.

6.3. Comparison between ARFEM and MCS-based RFEM

To validate the results obtained from ARFEM, a direct MCS-based RFEM run with 10,000 samples is carried out to calculate the P_f and R of the considered slope, where the fine FE model is directly used to perform deterministic slope stability analysis. The estimates of P_f and R are 3.20×10^{-3} and 7.00 m^3, respectively, as shown in Table 2. These results agree with those (i.e., 2.80×10^{-3} and 7.09 m^3) obtained from the target analysis in ARFEM because the same FE model is adopted. For comparison, Fig. 8 also shows the CDF and CRF obtained from MCS-based RFEM, which coincide with the target results of ARFEM for all *fs* values.

Table 1
Results of slope reliability and risk assessment using ARFEM.

k	Ω_k	$P(\Omega_k)$	Preliminary analysis			Target analysis		
			$P(F_p\|\Omega_k)$	$P_{f,p}$	R_p (m^3)	$P(F_t\|\Omega_k)$	$P_{f,t}$	R_t (m^3)
0	$1.274 \leqslant FS_p$	9×10^{-1}	0/450	8.84×10^{-4}	1.77	0/25	2.80×10^{-3}	7.09
1	$1.109 \leqslant FS_p < 1.274$	9×10^{-2}	0/450			0/25		
2	$1.005 \leqslant FS_p < 1.109$	9×10^{-3}	0/450			5/25		
3	$0.917 \leqslant FS_p < 1.005$	9×10^{-4}	392/450			25/25		
4	$FS_p < 0.917$	1×10^{-4}	50/50			25/25		

Table 2
Comparison of results between MCS-based RFEM and ARFEM.

Method		N_T		Time (day)[a]		P_f	COV(P_f)	R (m^3)	Unit COV
MCS-based RFEM		10,000		89.9		3.20×10^{-3}	0.18	7.00	18
ARFEM	Preliminary	1850	162[b]	0.3[c]	1.4[c]	2.80×10^{-3}[c]	0.31[c]	6.71[c]	3.9
	Target	125		1.1[c]					

[a] Estimated by parallel computing.
[b] $\xi \approx 1/50$ on average.
[c] Estimated on 20 independent runs.

These results indicate that ARFEM can produce consistent estimates of P_f and R compared with MCS-based RFEM.

Recall that only 125 fine FE analyses are required in ARFEM, which is much smaller than that (i.e., 10,000) required in MCS-based RFEM. Since the computational effort ratio ξ is about 1/50 on average, the equivalent sample size N_T of ARFEM calculated by Eq. (8) is 1850/50 + 125 = 162. In addition to the sample size, the COV of P_f is about $\sqrt{(1-P_f)/N_T P_f} = 0.18$ for MCS-based RFEM. Using 20 independent runs, the COV of P_f from ARFEM is about 0.31. To achieve a fair comparison of the computational efficiency, the unit COV [2] is taken as a measure of the computational efficiency in this study, which is defined as $\mathrm{COV}(P_f) \times \sqrt{N_T}$ and accounts for the effect of number of samples used in simulation on the variation of reliability estimate. As shown in Table 2, the unit COV values of MCS-based RFEM and ARFEM are 18 and 3.9, respectively. In other words, ARFEM only requires about 1/21 (i.e., $(3.9/18)^2$) of the computational effort for MCS-based RFEM to achieve the same computational accuracy. Physically, MCS-based RFEM takes about 89.9 days (about 3 months) to produce sufficiently accurate results on the same computer using parallel computing. The computational cost is too high for practitioners. In contrast, the total computational time of ARFEM is only about 1.4 days, acceptable for 3-D FE-based reliability analysis in practice. ARFEM significantly improves the computational efficiency of 3-D slope reliability analysis and risk assessment by incorporating the information obtained from preliminary analysis with coarse FE model into target analysis with fine FE model.

6.4. Correlation between coarse and fine FE models

Fig. 9 compares the *FS*, *V* and *L* of the selected 125 representative samples calculated by both coarse and fine FE models in Section 6.2, and illustrates the 1:1 lines and respective linear regression lines for reference. Although the linear regression lines do not overlap with the 1:1 lines, these FE responses are well correlated. The high correlations indicate that the coarse FE model used in preliminary analysis is appropriate and can reflect the main features, particularly the *FS*, of the fine FE model well. In addition, similar to deterministic slope stability analysis again, using coarse FE model generally leads to overestimation of *FS* and underestimation of *V* and *L*, which subsequently results in the underestimation of P_f and R. Such differences become more significant as responses increase.

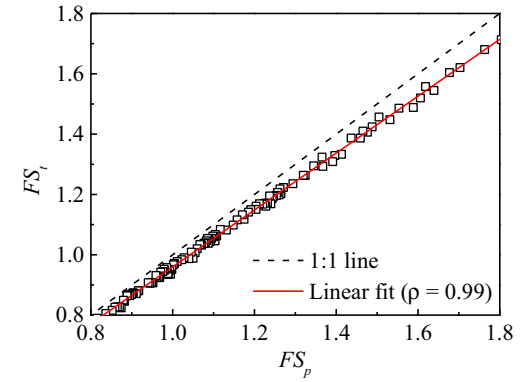

(a) Factor of safety, *FS*

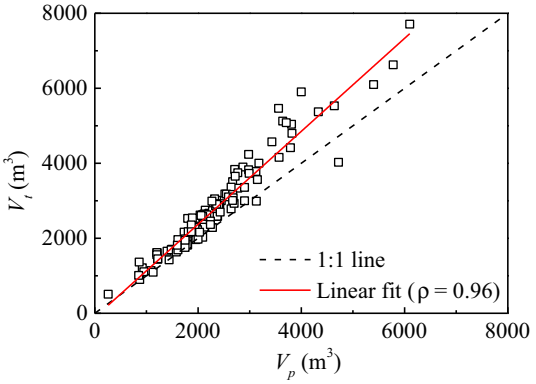

(b) Sliding mass volume, *V*

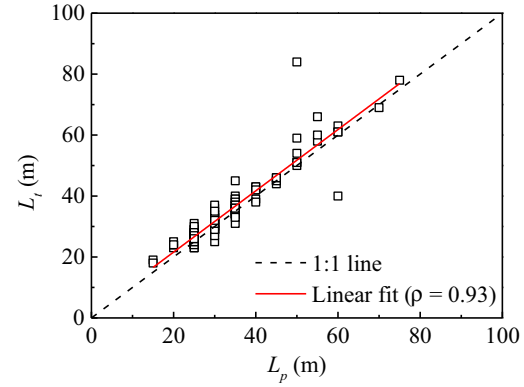

(c) Sliding mass length, *L*

Fig. 9. Comparison of FE responses obtained from coarse and fine FE models.

7. Effect of horizontal spatial variability on 3-D slope reliability and risk

With the aid of the improved computational efficiency provided by ARFEM, this section carries out a sensitivity study to explore the effect of horizontal spatial variability on 3-D slope reliability and risk. Five values of horizontal autocorrelation distance (i.e., l_h = 10 m, 20 m, 40 m, 80 m, and 120 m) are considered and the vertical autocorrelation distance l_v is taken as 2 m. For simplicity, all results presented in this section are obtained from target analysis in ARFEM.

Fig. 10(a) shows the slope failure probability and risk for different values of normalized horizontal autocorrelation distance (i.e., l_h/B). When l_h/B increases from 0.1 to 1.2, namely, the horizontal

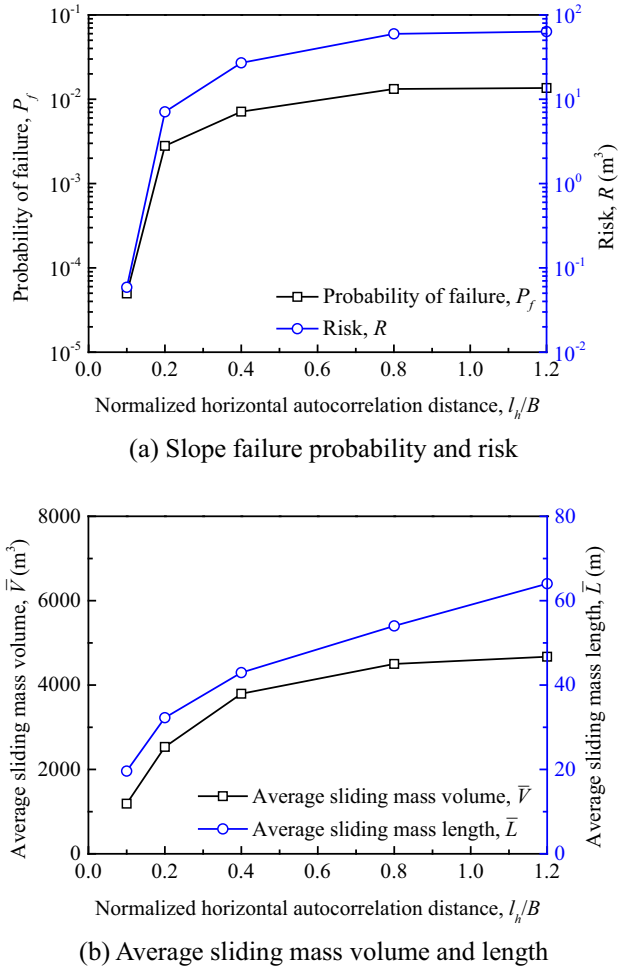

Fig. 10. Effect of horizontal spatial variability on results of slope failure.

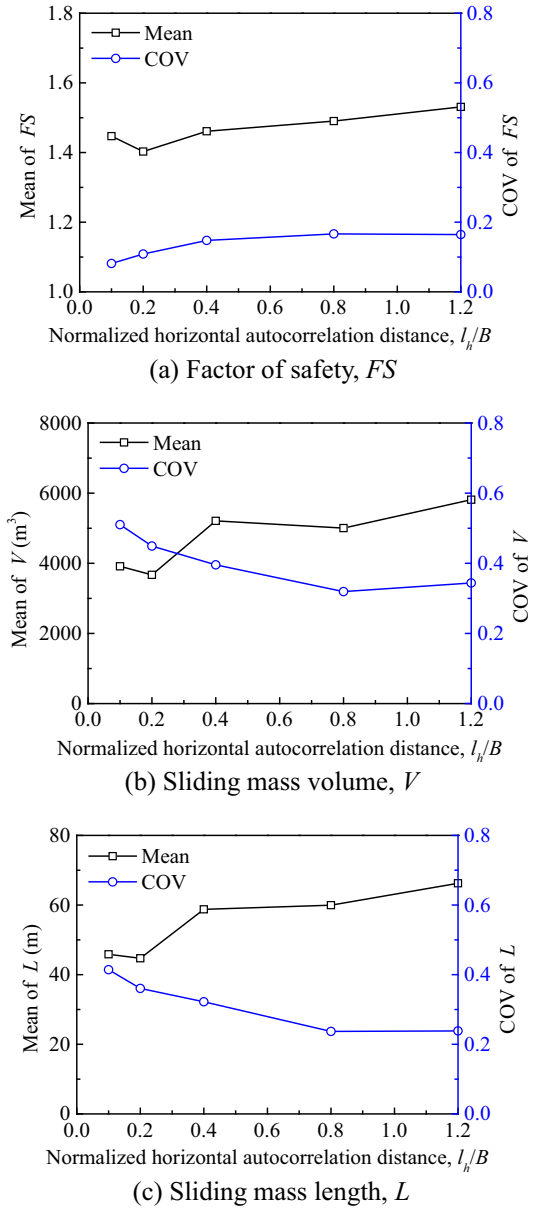

Fig. 11. Effect of horizontal spatial variability on FE responses of slope.

spatial variability becomes weaker, the estimated P_f and R significantly increase by about two and three orders of magnitude, respectively. The influence weakens when the horizontal autocorrelation distance exceeds half of the slope length (e.g., $l_h/B = 0.8$ and 1.2). Since the range of l_h is generally within 20–40 m, horizontal spatial variability will significantly affect P_f and R for long slopes, for instance, several kilometers long levees.

With respect to slope failure mechanisms, the average sliding mass volume $\bar{V}$ and average sliding mass length $\bar{L}$, evaluated by Eq. (5a) and failure samples, are shown in Fig. 10(b). As l_h/B increases from 0.1 to 1.2, $\bar{V}$ and $\bar{L}$ increase slightly in comparison with P_f and R. Note that $\bar{V}$ is equivalent to the average failure consequence $\bar{C}$ in this study. It can be concluded that R (i.e., $P_f \times \bar{C}$) is more sensitive to P_f than $\bar{C}$, similar to previous observation in 2-D slope risk assessment [31]. Additionally, $\bar{V}$ and $\bar{L}$ follow similar trends as l_h/B increases. This makes the average sliding mass area on the cross section (i.e., $E(V/L)$), which should be dominated by the lateral spatial variability, remain roughly unchanged. Thus, the horizontal spatial variability in the axial direction, instead of that in the lateral direction, affects 3-D slope failure mechanisms and average failure consequence.

Fig. 11 shows the effects of horizontal spatial variability on the mean and COV values of FS, V and L, which are evaluated using Eq. (5) and all random samples. As shown in Fig. 11(a), both mean and COV values of FS increase with increasing l_h. The increase in COV of FS leads to the increase in P_f. Fig. 11(b) and (c) shows that both the mean values of V and L increase and their COV values decrease as l_h increases. This implies that the number of possible failure modes along the axial direction reduces as the horizontal spatial variability weakens. For the extreme case that l_h becomes infinite, the 3-D slope is homogenous in the axial direction and can be simplified as a 2-D slope if the slope is long enough. This brings about only a few slope failure modes caused by the vertical spatial variability. Consequently, the COV values of V and L are minimal, and the corresponding mean values approach the results of the deterministic slope stability analysis.

Based on the aforementioned results, the horizontal spatial variability in the axial direction affects the failure mode, reliability and risk of 3-D slopes significantly, particularly for long slopes with relatively small horizontal autocorrelation distances (e.g., below half of the slope length). Such effects are properly incorporated into 3-D slope reliability analysis and risk assessment by ARFEM.

8. Summary and conclusion

This paper proposed an auxiliary random finite element method (ARFEM) for efficient three-dimensional (3-D) slope reliability analysis and risk assessment, and explored the effect of horizontal spatial variability on 3-D slope reliability and risk. A 3-D soil slope example was investigated to demonstrate the validity of ARFEM, and those results were verified by Monte Carlo Simulation-based RFEM. Several conclusions can be drawn:

(1) The proposed ARFEM not only provides reasonably accurate estimates of slope failure probability and risk, but also significantly reduces the computational effort, particularly at small probability levels. This benefits from the fact that ARFEM incorporates the information generated from preliminary analysis based on a coarse finite-element (FE) model into target analysis based on a fine FE model using response conditioning method. This can significantly enhance the applications of RFEM in geotechnical practice.
(2) 3-D slope probabilistic analysis (including both 3-D slope stability analysis and 3-D spatial variability modeling of soil properties) can reflect slope failure mechanism more realistically in terms of the shape, location and length of slip surface. With the 3-D FE analysis of slope stability, ARFEM provides a rigorous tool for 3-D slope probabilistic analysis, where 3-D spatial variability of soil properties is explicitly modeled.
(3) Horizontal spatial variability, particularly in the axial direction, might significantly influence the failure mode, reliability and risk of 3-D slopes, especially for long slopes with relatively small horizontal autocorrelation distances (e.g., below half of the slope length). These effects can be properly incorporated into 3-D slope reliability analysis and risk assessment using ARFEM.

Although the coarse and fine FE models used in this study differ in their mesh size only, the proposed method applies generally to a coarse FE model with simplified soil constitutive model, large time-step, or any other techniques to improve the efficiency of deterministic FE analysis.

Acknowledgments

This work was supported by the National Science Fund for Distinguished Young Scholars (Project No. 51225903), the National Basic Research Program of China (973 Program) (Project No. 2011CB013502), the National Natural Science Foundation of China (Project Nos. 51329901, 51579190, 51528901), and the Natural Science Foundation of Hubei Province of China (Project No. 2014CFA001).

References

[1] Ang AH-S, Tang WH. Probability concepts in engineering: emphasis on applications to civil and environmental engineering. 2nd ed. Hoboken, New Jersey: John Wiley & Sons; 2007.
[2] Au SK. Augmenting approximate solutions for consistent reliability analysis. Probab Eng Mech 2007;22(1):77–87.
[3] Au SK, Beck JL. Estimation of small failure probabilities in high dimensions by subset simulation. Probab Eng Mech 2001;16(4):263–77.
[4] Au SK, Wang Y. Engineering risk assessment with subset simulation. Singapore: John Wiley & Sons; 2014.
[5] Cao Z, Wang Y. Bayesian model comparison and selection of spatial correlation functions for soil parameters. Struct Saf 2014;49:10–7.
[6] Cao Z, Wang Y, Li DQ. Quantification of prior knowledge in geotechnical site characterization. Eng Geol 2016;203:107–16.
[7] Chen HX, Zhang S, Peng M, Zhang LM. A physically-based multi-hazard risk assessment platform for regional rainfall-induced slope failures and debris flows. Eng Geol 2016;203:15–29.
[8] Ching JY, Wang JS. Application of the transitional Markov chain Monte Carlo algorithm to probabilistic site characterization. Eng Geol 2016;203:151–67.
[9] Dassault Systèmes. Abaqus unified FEA; 2015. <http://www.3ds.com/products-services/simulia/portfolio/abaqus/latest-release/>.
[10] Griffiths DV, Lane PA. Slope stability analysis by finite elements. Geotechnique 1999;49(3):387–403.
[11] Griffiths DV, Fenton GA. Probabilistic slope stability analysis by finite elements. J Geotech Geoenviron Eng 2004;130(5):507–18.
[12] Griffiths DV, Marquez RM. Three-dimensional slope stability analysis by elasto-plastic finite elements. Geotechnique 2007;57(6):537–46.
[13] Griffiths DV, Marquez RM. Discussion: three-dimensional slope stability analysis by elasto-plastic finite elements. Geotechnique 2008;58(8):683–5.
[14] Griffiths DV, Huang J, Fenton GA. On the reliability of earth slopes in three dimensions. Proc Roy Soc Lond A: Math, Phys Eng Sci 2009;465(2110):3145–64.
[15] Hicks MA, Spencer WA. Influence of heterogeneity on the reliability and failure of a long 3D slope. Comput Geotech 2010;37(7):948–55.
[16] Hicks MA, Nuttall JD, Chen J. Influence of heterogeneity on 3D slope reliability and failure consequence. Comput Geotech 2014;61:198–208.
[17] Huang J, Lyamin AV, Griffiths DV, Krabbenhoft K, Sloan SW. Quantitative risk assessment of landslide by limit analysis and random fields. Comput Geotech 2013;53:60–7.
[18] Jamshidi Chenari R, Alaie R. Effects of anisotropy in correlation structure on the stability of an undrained clay slope. Georisk 2015;9(2):109–23.
[19] Ji J, Low BK. Stratified response surfaces for system probabilistic evaluation of slopes. J Geotech Geoenviron Eng 2012;138(11):1398–406.
[20] Ji J. A simplified approach for modelling spatial variability of undrained shear strength in out-plane failure mode of earth embankment. Eng Geol 2014;183:315–23.
[21] Ji J, Chan CL. Long embankment failure accounting for longitudinal spatial variation – a probabilistic study. Comput Geotech 2014;61:50–6.
[22] Jiang SH, Li DQ, Cao ZJ, Zhou CB, Phoon KK. Efficient system reliability analysis of slope stability in spatially variable soils using Monte Carlo Simulation. J Geotech Geoenviron Eng 2015;141(2):04014096.
[23] Jiang SH, Li DQ, Zhang LM, Zhou CB. Slope reliability analysis considering spatially variable shear strength parameters using a non-intrusive stochastic finite element method. Eng Geol 2014;168:120–8.
[24] Kasama K, Whittle AJ. Effect of spatial variability on the slope stability using random field numerical limit analyses. Georisk 2016;10(1):42–54.
[25] Le TMH. Reliability of heterogeneous slopes with cross-correlated shear strength parameters. Georisk 2014;8(4):250–7.
[26] Li CC, Der Kiureghian A. Optimal discretization of random fields. J Eng Mech 1993;119(6):1136–54.
[27] Li DQ, Chen YF, Lu WB, Zhou CB. Stochastic response surface method for reliability analysis of rock slopes involving correlated non-normal variables. Comput Geotech 2011;38(1):58–68.
[28] Li DQ, Qi XH, Phoon KK, Zhang LM, Zhou CB. Effect of spatially variable shear strength parameters with linearly increasing mean trend on reliability of infinite slopes. Struct Saf 2014;49:45–55.
[29] Li DQ, Jiang SH, Cao ZJ, Zhou W, Zhou CB, Zhang LM. A multiple response-surface method for slope reliability analysis considering spatial variability of soil properties. Eng Geol 2015;187:60–72.
[30] Li DQ, Zhang L, Tang XS, Zhou W, Li JH, Zhou CB, et al. Bivariate distribution of shear strength parameters using copulas and its impact on geotechnical system reliability. Comput Geotech 2015;68:184–95.
[31] Li DQ, Xiao T, Cao ZJ, Zhou CB, Zhang LM. Enhancement of random finite element method in reliability analysis and risk assessment of soil slopes using subset simulation. Landslides 2016;13:293–303.
[32] Li DQ, Xiao T, Cao ZJ, Phoon KK, Zhou CB. Efficient and consistent reliability analysis of soil slope stability using both limit equilibrium analysis and finite element analysis. Appl Math Model 2016;40(9–10):5216–29.
[33] Li DQ, Zheng D, Cao ZJ, Tang XS, Phoon KK. Response surface methods for slope reliability analysis: review and comparison. Eng Geol 2016;203:3–14.
[34] Li DQ, Qi XH, Cao ZJ, Tang XS, Phoon KK, Zhou CB. Evaluating slope stability uncertainty using coupled Markov chain. Comput Geotech 2016;73:72–82.
[35] Li L, Wang Y, Cao Z. Probabilistic slope stability analysis by risk aggregation. Eng Geol 2014;176:57–65.
[36] Li YJ, Hicks MA, Nuttall JD. Comparative analyses of slope reliability in 3D. Eng Geol 2015;196:12–23.
[37] Lloret-Cabot M, Fenton GA, Hicks MA. On the estimation of scale of fluctuation in geostatistics. Georisk 2014;8(2):129–40.
[38] Phoon KK, Kulhawy FH. Characterization of geotechnical variability. Can Geotech J 1999;36(4):612–24.
[39] Phoon KK, Ching JY. Risk and reliability in geotechnical engineering. Singapore: Taylor and Francis; 2014.
[40] Pradlwarter HJ, Schuëller GI. Local domain Monte Carlo simulation. Struct Saf 2010;32(5):275–80.
[41] Santoso AM, Phoon KK, Quek ST. Effects of soil spatial variability on rainfall-induced landslides. Comput Struct 2011;89(11):893–900.
[42] Sudret B, Der Kiureghian A. Stochastic finite element methods and reliability: a state-of-the-art report. Department of Civil and Environmental Engineering, University of California; 2000.

[43] Schuëller GI, Pradlwarter HJ, Koutsourelakis PS. A critical appraisal of reliability estimation procedures for high dimensions. Probab Eng Mech 2004;19(4):463–74.
[44] Tang XS, Li DQ, Rong G, Phoon KK, Zhou CB. Impact of copula selection on geotechnical reliability under incomplete probability information. Comput Geotech 2013;49:264–78.
[45] Tang XS, Li DQ, Zhou CB, Phoon KK. Copula-based approaches for evaluating slope reliability under incomplete probability information. Struct Saf 2015;52:90–9.
[46] Vanmarcke EH. Reliability of earth slopes. J Geotech Eng Divis 1977;103 (12):1247–65.
[47] Vanmarcke EH. Risk of limit-equilibrium failure of long earth slopes: how it depends on length. In: Geotechnical risk assessment & management (GeoRisk 2011), Atlanta, Georgia, United States; June 26–28, 2011. p. 1–24. http://dx.doi.org/10.1061/41183(418)1.
[48] Vanmarcke EH. Random fields: analysis and synthesis. revised and expanded new ed. Singapore: World Scientific Publishing Co., Pte. Ltd.; 2010.
[49] Vorechovsky M. Simulation of simply cross correlated random fields by series expansion methods. Struct Saf 2008;30(4):337–63.
[50] Wang Y, Cao Z, Au SK. Efficient Monte Carlo simulation of parameter sensitivity in probabilistic slope stability analysis. Comput Geotech 2010;37 (7):1015–22.
[51] Wang Y, Cao Z, Au SK. Practical reliability analysis of slope stability by advanced Monte Carlo Simulations in a spreadsheet. Can Geotech J 2011;48 (1):162–72.
[52] Wang Y, Cao Z, Li D. Bayesian perspective on geotechnical variability and site characterization. Eng Geol 2016;203:117–25.
[53] Xiao T, Li DQ, Cao ZJ, Tang XS. Non-intrusive reliability analysis of multi-layered slopes in spatially variable soils. In: Schweckendiek T et al., editor. Fifth international symposium on geotechnical safety and risk (ISGSR 2015), Rotterdam, The Netherlands, October 13–16, 2015. Geotechnical safety and risk V; 2015. p. 184–90.
[54] Zhu H, Zhang LM, Zhang LL, Zhou CB. Two-dimensional probabilistic infiltration analysis with a spatially varying permeability function. Comput Geotech 2013;48:249–59.